Clim Dyn (2018) 50:1659–1673
DOI 10.1007/s00382-017-3713-y

Association between mean and interannual equatorial Indian Ocean subsurface temperature bias in a coupled model

G. Srinivas[1,2] · Jasti S. Chowdary[1] · C. Gnanaseelan[1] · K. V. S. R. Prasad[2] · Ananya Karmakar[1,3] · Anant Parekh[1]

Received: 8 February 2017 / Accepted: 26 April 2017 / Published online: 3 May 2017

Abstract In the present study the association between mean and interannual subsurface temperature bias over the equatorial Indian Ocean (EIO) is investigated during boreal summer (June through September; JJAS) in the National Centers for Environmental Prediction (NCEP) Climate Forecast System (CFSv2) hindcast. Anomalously high subsurface warm bias (greater than 3 °C) over the eastern EIO (EEIO) region is noted in CFSv2 during summer, which is higher compared to other parts of the tropical Indian Ocean. Prominent eastward current bias in the upper 100 m over the EIO region induced by anomalous westerly winds is primarily responsible for subsurface temperature bias. The eastward currents transport warm water to the EEIO and is pushed down to subsurface due to downwelling. Thus biases in both horizontal and vertical currents over the EIO region support subsurface warm bias. The evolution of systematic subsurface warm bias in the model shows strong interannual variability. These maximum subsurface warming episodes over the EEIO are mainly associated with La Niña like forcing. Strong convergence of low level winds over the EEIO and Maritime continent enhanced the westerly wind bias over the EIO during maximum warming years. This low level convergence of wind is induced by the bias in the gradient in the mean sea level pressure with positive bias over western EIO and negative bias over EEIO and parts of western Pacific. Consequently, changes in the atmospheric circulation associated with La Niña like conditions affected the ocean dynamics by modulating the current bias thereby enhancing the subsurface warm bias over the EEIO. It is identified that EEIO subsurface warming is stronger when La Niña co-occurred with negative Indian Ocean Dipole events as compared to La Niña only years in the model. Ocean general circulation model (OGCM) experiments forced with CFSv2 winds clearly support our hypothesis that ocean dynamics influenced by westerly winds bias is primarily responsible for the strong subsurface warm bias over the EEIO. This study advocates the importance of understanding the ability of the models in representing the large scale air–sea interactions over the tropics and their impact on ocean biases for better monsoon forecast.

Keywords Subsurface temperature · Coupled model · Indian Ocean · La Niña · SST

1 Introduction

The tropical Indo-Pacific Ocean plays a significant role in modulating the climate over the different parts of the globe (e.g., Chang et al. 2006; Preethi et al. 2015). A semi-annual wind forcing over the tropical Indian Ocean (TIO) with the southwest and northeast monsoon winds (e.g., Pant and Rupa Kumar 1997; Sengupta et al. 2004) is important in determining the upper ocean circulation (e.g., McCreary et al. 1993; Schott and McCreary 2001; Shankar et al. 2002). In the equatorial Indian Ocean (EIO), the surface currents reverse their directions four times a year. During boreal winter equatorial currents flow westward, strongly eastward during spring and fall and the currents

✉ Jasti S. Chowdary
jasti@tropmet.res.in

[1] Indian Institute of Tropical Meteorology (IITM), Pune 411 008, India

[2] Department of Meteorology and Oceanography, Andhra University, Visakhapatnam 530 003, India

[3] Department of Atmospheric and Space Sciences, Savitribai Phule Pune University, Pune 411 007, India

flow (weak) westward during summer (e.g., Wyrtki 1973; Schott et al. 2009; Sengupta et al. 2007). Surface and subsurface temperature in general is warmer over the Eastern EIO (EEIO) as compared to western EIO in boreal summer. Cold water advection from southern Indian Ocean and upwelling induced by strong cross equatorial monsoon flow keeps western EIO (surface and subsurface temperature) cooler than EEIO (e.g., Saji et al. 1999; Anderson et al. 2002).

Surface and subsurface temperature and upper ocean heat content over the Indian Ocean region are known to influence the Indian Summer Monsoon (ISM) rainfall, climate over the Maritime continent, Australia, East Asia and Africa (e.g., Krishnamurthy and Kinter 2003; Krishnan et al. 2006; Cherchi and Navarra 2007). Importance of subsurface temperature variations in influencing the climate variability and change are reported in the literature (e.g., Xie et al. 2002; Ruiz et al. 2005; Schott et al. 2009). Further subsurface temperature variations have potential impact on tropical cyclones and depressions etc (e.g., Balaguru et al. 2013; Sreenivas and Gnanaseelan 2014; Vincent et al. 2014). Hence, one of the important concerns in coupled models is the accurate representation of subsurface and surface features over the tropical regions. On the other hand, anomalous ocean–atmosphere phenomenon such as El Niño–Southern Oscillation (ENSO) and Indian Ocean Dipole (IOD) may also contribute to upper ocean mean bias in coupled models. For example Tao et al. (2015) pointed out that sea surface temperature (SST) bias in many coupled models associated with El Niño modulates rainfall, which in turn affects atmospheric circulation and consequently the oceanic processes. This indicates that the misrepresentation of interannual upper ocean variability could influence the climatic anomalies over Indo-Pacific region.

Indian Ocean subsurface temperature plays a major role in modulating the air–sea interaction processes over the Indo-Pacific domain (Yamagata et al. 2004; Luo et al. 2012). Large upper ocean bias in coupled models over the equatorial region influences the predictability of rainfall both locally and remotely (e.g., Kirtman and Vecchi 2011; Luo et al. 2005; Chowdary et al. 2015). Subsurface ocean temperature biases are known to have large impact on sea level changes, the ocean circulation (e.g., Large and Danabasoglu 2006; Brown et al. 2013) and the Bjerknes feedback (e.g., Keenlyside and Latif 2007). Many Coupled Model Intercomparison Project Phase 5 (CMIP5) models display IOD like pattern in SST biases with strong subsurface cold (warm) biases in the east (west) EIO in summer (Li et al. 2015a). They pointed out the importance of interaction between monsoon circulation and subsurface bias in EIO region. Further Li et al. (2015b) demonstrated that a too deep thermocline dome (positive bias) weakens the influence of subsurface variability on SST and limits skills in many CMIP5 models. This motivated us to examine the summer time subsurface temperature bias in the forecast model National Centers for Environmental Prediction (NCEP) Climate Forecast System version-2 (CFSv2; Saha et al. 2014), which is currently used for monsoon forecast in many countries including India (http://www.tropmet.res.in/monsson/index.php). Our analysis suggests that CFSv2 displays a strong subsurface temperature warm bias over EEIO unlike in CMIP5 models. The current understating of the relationship between the subsurface temperature and atmospheric circulation is a challenging task for the modelling community. Chowdary et al. (2016b) studied processes responsible for annual mean subsurface temperature bias in long-term CFSv2 free run over the entire TIO. Such study for CFSv2 hindcast run is long pending. Further previous studies did not look at the structure and interannual variability of seasonal subsurface temperature bias. In the Indian monsoon prospective, it is essential to investigate the model biases in summer season especially in the hindcasts or forecasts in CFSv2 (e.g., Saha et al. 2016). This part of the ocean has strong influence on the atmosphere and the active convection sustains over this region for most of the year (e.g., Schott et al. 2009). Of particular interest is the attribution of model biases to coupled processes and the upper ocean currents.

Rest of the paper is organized as follows. Section 2 gives the detailed information about model setup and methodology adopted to generate hindcast and other datasets used. Sensitivity experiments carried out by Ocean General Circulation Model (OGCM) are also presented in this section. Section 3 addresses the temperature biases over the equatorial Indian Ocean, and Sect. 4 discusses the interannual subsurface temperature biases. Finally Sect. 5 provides the summary and conclusions.

2 Model and data used

The fully coupled ocean–atmosphere model NCEP-CFSv2 is the advanced version of CFSv1 (Saha et al. 2006, 2014). NCEP global forecast system (GFS) is the atmospheric component with 64 sigma layers vertically and T126 (~100 km) horizontal resolution. The oceanic component is the Modular Ocean Model version 4 (MOM4P0) (Griffies et al. 2004) with horizontal resolution of 0.25° in the 10°S–10°N latitude bandwidth and 0.5° resolution elsewhere and 40 vertical levels. The CFSv2 retrospective forecast (hindcast) is prepared for 9 months and covering a period of 30 years from 1985 to 2014 at Indian Institute of Tropical Meteorology (IITM). The atmospheric initial conditions are obtained from the NCEP Reanalysis (R2) data (Saha et al. 2010). The ocean initial conditions are obtained from the NCEP Global Ocean Data Assimilation System.

Retrospective forecast starts from a specific month May, there are ten atmospheric initial conditions (ten ensemble members) that are partitioned into two segments. The first set uses five atmospheric initial states of the 1st, 2nd, 3rd, 4th and 5th of May and uses the same pentad ocean initial condition centred on the 3rd of the same month. The second set uses the five atmospheric initial states of the 6th, 7th, 8th, 9th and 10th of May and the same pentad ocean initial condition centred on the 8th of May. For the analysis, we have utilized ensemble mean forecasts obtained by averaging the above ten ensemble members. It is important to note that in this study we have examined the subsurface temperature bias only during boreal summer (JJAS). CFSv2 ocean component is evaluated against Met Office Hadley Centre observations datasets (Hadley EN4.1.1) temperature for the period 1985–2014 (http://www.metoffice.gov.uk/hadobs/en4/download-en4-1-1.html) (Good et al. 2013) and Estimating the Circulation and Climate of the Ocean (ECCO-2) three dimensional ocean currents covering a period 1992–2013 (Wunsch and Heimbach 2013). European Centre for Medium-Range Weather Forecasts (ECMWF) reanalysis (ERA-Interim; Dee et al. 2011) surface, 850 and 200 hPa level winds and mean sea level pressure (MSLP) and CPC merged analysis of precipitation (CMAP; Xie and Arkin 1997) are utilized in the present study.

The OGCM used to perform sensitivity experiments in this study is the Geophysical Fluid Dynamics Laboratory (GFDL) Modular Ocean Model Version 5 (MOM5) (Griffies 2012). MOM5 is a global model having 50 vertical levels. It has a constant zonal resolution of 1° and meridional resolution varying from 0.33° at equator to 0.67° up to tropics and gradually increasing to 1° towards pole. The upper ocean mixed layer and thermocline zones are well resolved in the model with 20 vertical levels within a depth of 200 m. The vertical resolution gradually changes to maximum thickness of 371 m at a depth of 5000 m. The model has been provided with realistic topography of 0.5° resolution, which is derived from the 5-min global topography from ETOPO5 (Earth Topography-5 min) database. The model is spun up for 50 years with climatological forcing of downwelling shortwave and long wave radiation, 10 m surface wind fields, specific humidity, air temperature, surface pressure and surface precipitation etc. from coordinated ocean–ice reference experiments (CORE) version 2. This model was initialized using the annual climatologies of temperature and salinity from Levitus et al. (1998). Details of model experiments are provided below.

To test the impact of EIO winds and current bias on subsurface temperature bias, we have carried out a couple of OGCM sensitivity experiments by changing surface wind forcing. In the first experiment (Exp-1) composite of strong warm years (ERA-Interim) surface wind forcing is used to run the ocean model and in the second experiment (Exp-2) similar composite of winds obtained from CFSv2 are used. Rest of the required model forcing has been taken from the climatological CORE2. Forcing such as daily shortwave and longwave radiation, 6 hourly specific humidity, air temperature and sea level pressure and monthly surface precipitation and annual cycle of river runoff are kept same for both experiment.

3 Temperature biases over the EIO during boreal summer

This section discusses the mean bias of surface and subsurface temperature in CFSv2 over the TIO with special emphasis on EEIO region during boreal summer monsoon (JJAS). It is important to note that the spatial patterns of mean precipitation, SST and surface and 850 hPa winds in CFSv2 are consistent with the observations over the TIO (Fig. 1). Spatial distribution of precipitation reveals that the model rainfall is overestimated over the eastern Bay of Bengal, western parts of Indian subcontinent and some parts of the TIO (Fig. 1a, b). Most prominently low level winds over the EIO are slightly stronger in CFSv2 compared to the observations. Such kind of surface wind bias may directly affect the upper ocean temperature bias (e.g., Li et al. 2015a; Chowdary et al. 2016a).

To quantify the difference between CFSv2 and observations; bias for SST, surface winds, surface currents (averaged over the upper 50 m depth), precipitation, subsurface temperature (averaged over a depth of 120–140 m as the maximum bias in subsurface temperature is found between 120 and 140 m depth) and heat content of the upper ocean (surface to a depth of 150 m) are displayed in Fig. 2. Model SST shows cold bias over most of the TIO and strong warm bias in the subsurface over EEIO by more than 2 °C (Fig. 2a, b), which is consistent with previous studies (e.g. Chowdary et al. 2016b). The magnitude of the model SST is underestimated over western Arabian Sea and western EIO and in the off equatorial region over the central Indian Ocean as compared to the observations (Fig. 2a). On the other hand the SST bias in the EEIO region displays weak positive bias. Analogous to subsurface temperature bias, thermocline depth (D20) also displays strong bias in many parts of the basin including EEIO (Fig. 2b). Warm bias in the upper ocean heat content over the EEIO suggests the dominant contribution of subsurface bias on heat continent (Fig. 2c). The SST gradient between eastern and western EIO is 1.4 and 2 °C in the observations and model respectively. This stronger gradient in the model may affect the ocean–atmosphere feedback mechanisms over EIO. Thus addressing the possible causes for these subsurface temperature biases is crucial not only because it helps to

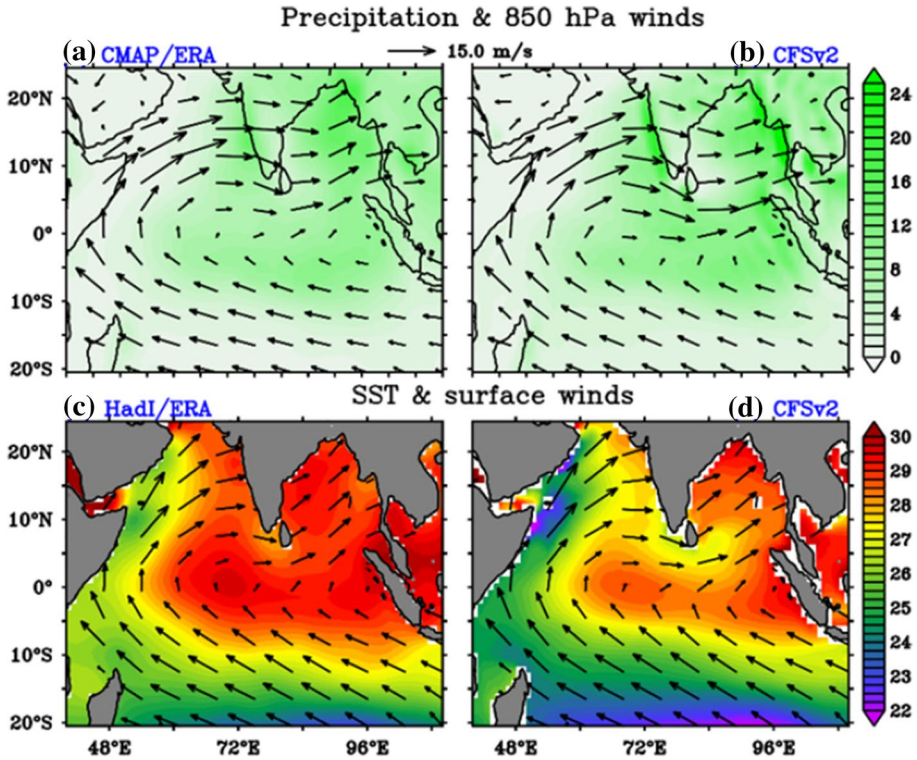

Fig. 1 JJAS mean: **a** precipitation (CMAP, *shaded*; mm/day) and 850 hPa winds (ERA-Interim, *vectors*; m/s), **b** same as in **a** but for CFSv2, **c** SST (HadI EN4, *shaded*; °C) and surface winds (ERA-Interim, vectors; m/s) and **d** same as in **c** but for CFSv2 (initialized in May)

understand the surface biases but it may also help in unravelling the causes of dry biases in precipitation over Indian land mass. So this problem remains as an important issue in the coupled modelling framework.

Surface cold bias in the model is mainly attributed to excess heat loss to atmosphere due to anomalous dry atmospheric humidity (away from equator) (e.g., Pokhrel et al. 2012; De et al. 2015) and partly due to deeper than the observed mixed layer (e.g., Jiang et al. 2013). Cold SST biases over the global tropics are reported in many CMIP5 models (Li and Xie 2012, 2014) and are attributed to the overestimation of cloud amount (Lin 2007; Li and Xie 2012). On the other hand, equatorial biases are influenced by biases in wind forcing and resultant ocean dynamics (e.g., Chowdary et al. 2016a). Surface wind shows westerly wind bias over EIO (Fig. 2d) and in response to this wind bias, eastward current bias is evident in the upper 50 m (Fig. 2d, e). These currents assist in piling up of water in the EEIO and deepen the thermocline, supporting warm bias at subsurface (Fig. 2b, e). Over the southeastern tropical Indian Ocean, anti-cyclonic bias in currents is apparent. Recent studies (Li et al. 2015a, 2016) suggest that most of CMIP5 CGCMs (coupled general circulation model) feature equatorial easterly surface wind bias along the equatorial Indian Ocean, inducing too cool subsurface temperature in the EEIO. However, CFSv2 displays strong westerly wind bias and EEIO subsurface warm bias unlike in many CMIP5 models (figure not shown), suggesting the unique feature in the model. Li et al. (2015a) attributed the Indian summer monsoon circulation with weak cross-equatorial flow as origin of such equatorial easterly wind biases in CMIP5 CGCMs. In case of CFSv2 strong southerly cross-equatorial wind over the western Indian Ocean is noted along with equatorial westerly winds bias (Fig. 2d). This strong cross equatorial flow is favourable for positive precipitation anomalies over Western Ghats (Fig. 2f), through enhanced moisture transport. Similarly strong westerly wind bias along EIO supports warming of EEIO surface and subsurface temperature. Apart from this the surface cooling and subsurface warming in CFSv2 indicate a weakened thermal stratification in the EEIO region. Chowdary et al. (2016b) suggested that weak stability of the upper ocean and high vertical shear of horizontal current in CFSv2 compared to the observations could play a crucial role in the subsurface warm bias over EIO region. Warm temperature over EEIO supports local convection and subsidence over the head Bay of Bengal region and reduces rainfall in the latter region (Fig. 2f). Convergence of low level winds and upper ocean heat content bias over EEIO support positive rainfall bias locally (Fig. 2f), which affects the monsoon rainfall over India.

Depth–longitude plot of temperature bias averaged between 3°N and 3°S over the Indian Ocean is illustrated in Fig. 3a. Strong subsurface warm bias in the entire EIO is seen with maximum bias in the east. Upper 60 m on the other hand displays cold bias. This surface and subsurface

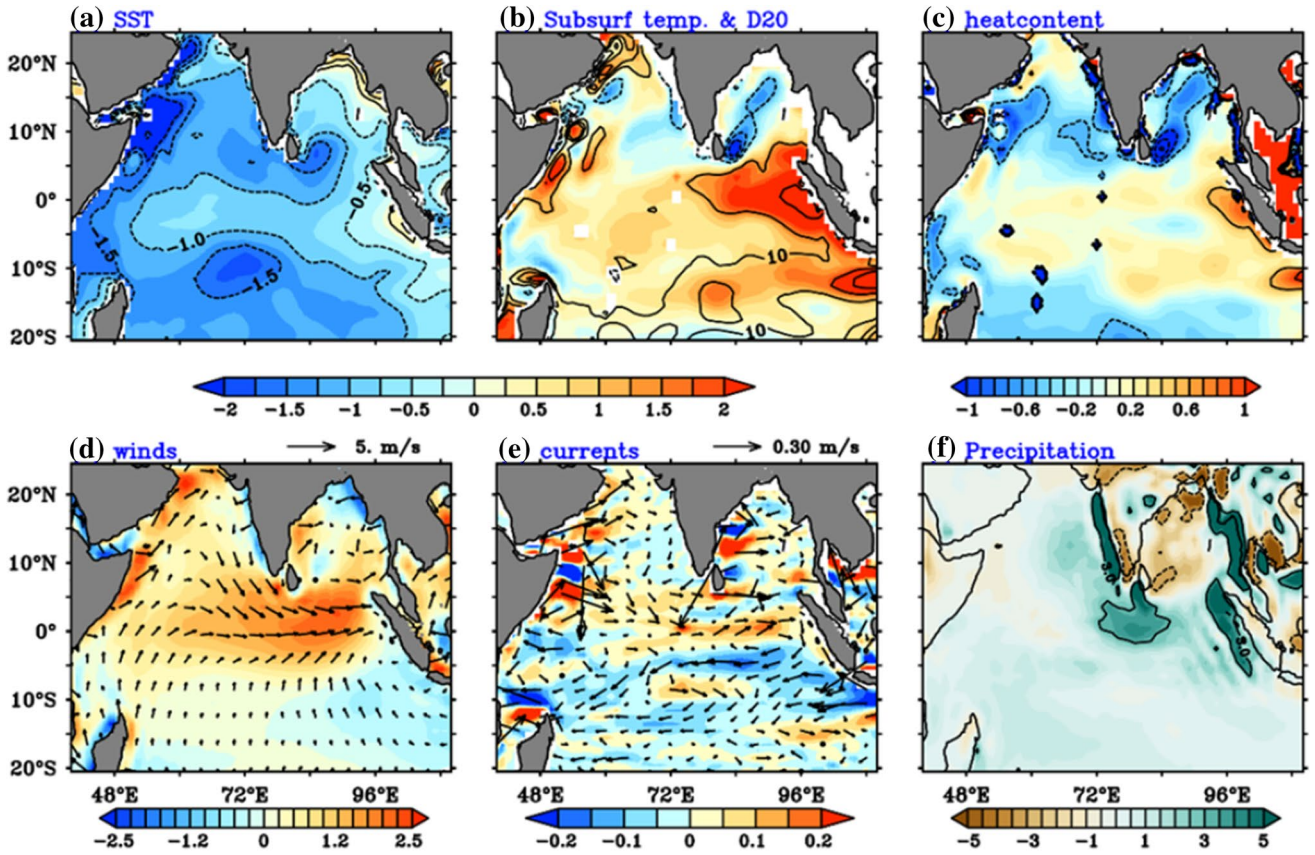

Fig. 2 JJAS mean bias: **a** SST (*shaded* and contour; °C) and **b** subsurface temperature averaged over a depth of 120–140 m (*shaded*; °C) and thermocline depth (D20, contour; m), and **c** heat content of upper 150 m depth (*shaded* and *contour*; °C), **d** zonal wind component (*shaded*; m/s) and surface winds (vectors; m/s), **e** zonal current (*shaded*; m/s) and surface currents (vectors; m/s) averaged upper 50 m depth and **f** precipitation (*shaded* and *contour*; mm/day). Bias is calculated as difference between CFSv2 and HadI EN4, ERA-Interim winds, ECCO2 currents and CMAP precipitation

temperature biases are consistent with the eastward current bias in the upper ocean (80 m) and westward current bias below. These zonal current biases are accompanied by vertical current bias with downward (upward) flow in the eastern (western) EIO (Fig. 3a, c). ECCO mean zonal current for summer shows eastward current in the upper 60 m with westward current below (Fig. 3b). Bias in vertical component of the current shows downward motion over the EEIO extending up to 100 m depth. This indicates downwelling of warm waters to subsurface layers (Fig. 3d). Thus, bias in subsurface temperature over the EIO is mostly consistent with ocean current and winds bias. Further, the contribution of interannual variability on this summer mean ocean temperature bias in CFSv2 is explored.

4 Interannual subsurface temperature biases

Depth–time plot of temperature bias averaged over the EEIO (90–100°E and 5°S–5°N) for JJAS is illustrated in Fig. 4a. It is clear that subsurface warm bias is not similar in all the years. Anomalously warm subsurface episodes are seen in different years with deeper D20. Time series obtained by averaging maximum subsurface temperature bias over EEIO from 120 to 140 m depth is displayed in Fig. 4b. Time series of EEIO subsurface temperature bias revealed that years like 1988, 1989, 1998, 1999, 2000, 2003, 2007 and 2011 displayed warm bias episodes (Fig. 4b). The warm bias years are selected if the index is more than two standard deviation (>2 °C). Further model Niño 3.4 and dipole mode index (DMI) for SST anomaly is displayed in Fig. 4c. Correlation between the observations and model Niño 3.4 (DMI) is 0.8 (0.32), suggesting that CFSv2 has high (low) skill representing ENSO (IOD) (e.g., Chaudhari et al. 2013; Ramu et al. 2016). It is clear from Niño 3.4 that all the warm subsurface bias episodes are co-occurred with negative SST anomaly episodes in the eastern Pacific (Fig. 4c). Correlation between subsurface temperature and Niño3.4 region SST anomalies is −0.68 and it is statistically significant at 95% level.

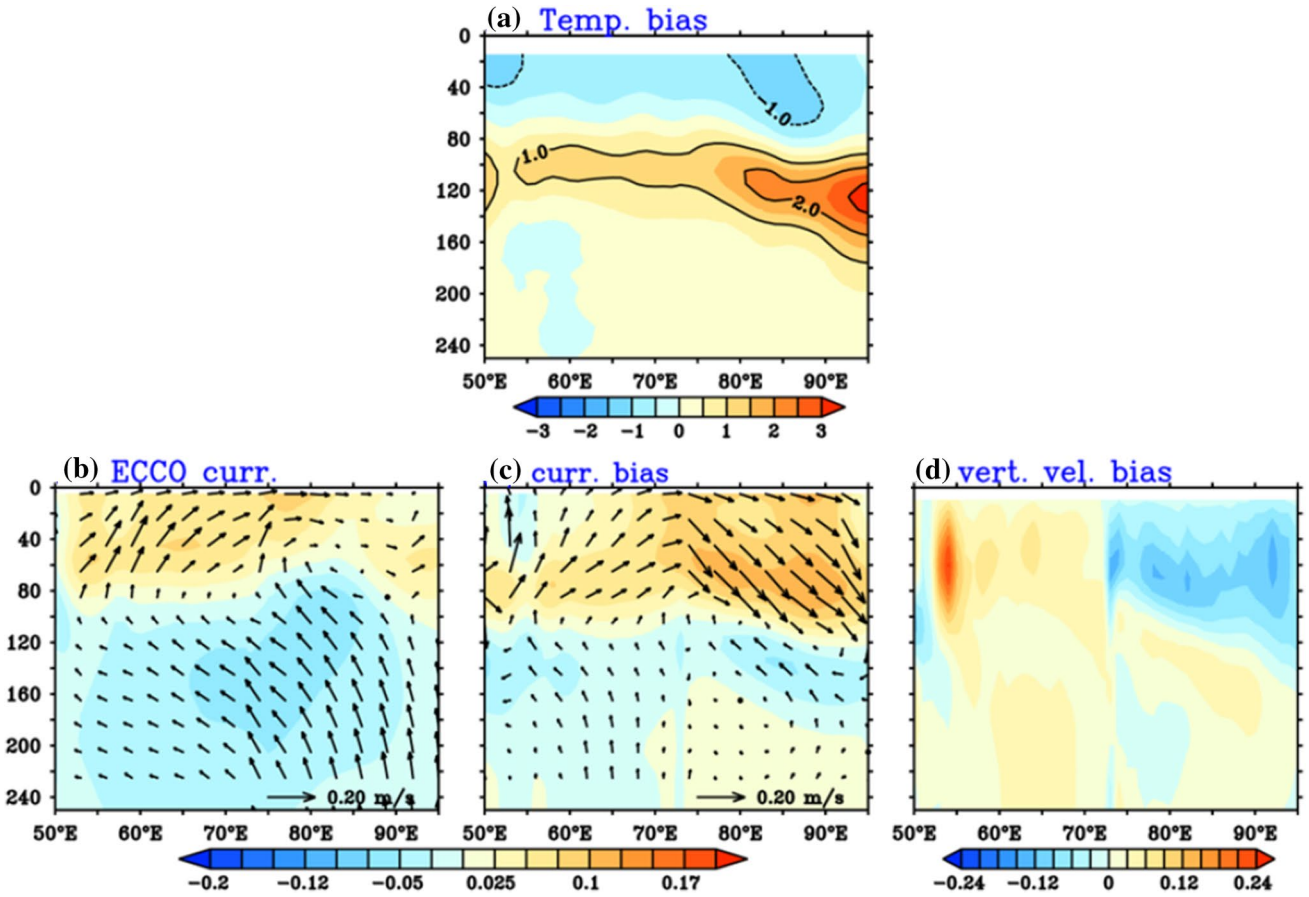

Fig. 3 **a** Depth–longitude plot (JJAS) for upper 250 m (average over 3°S–3°N) temperature bias (*shaded* and *contour*; °C) and **b** ECCO mean zonal current (*shaded*; m/s), and zonal and vertical currents (10^4 m/s) (vectors; m/s), and **c** same as **b** but for bias (CFSv2 minus ECCO), and **d** bias for vertical current (*shaded*; 10^4 m/s). Bias is calculated from ECCO2 and HadI EN4

Spatial distribution of SST anomaly composite of above mentioned years shows a La Niña like pattern in both the observations and model (Fig. 4d). Note that large scale pattern and subsurface temperature bias over EEIO region is similar for developing La Niña (1988, 1998 and 2007) and decaying La Niña (1989, 1999, 2000 and 2011) cases (figure not shown), thus we have considered composite of all warm years for further analysis and hereafter referred as strong warm years or La Niña like years. It is well established that ENSO is the most energetic climate signal after the seasonal cycle, the major source of interannual variability worldwide and a dominant driver of climate teleconnections (e.g., Ballester et al. 2013; Krishnamurthy and Kirtman 2003). This study suggests that this energetic climate signal in coupled models contributed for the upper ocean biases remotely elsewhere. Composite of maximum warm year SST anomalies displays very weak negative IOD signals both in the model and observations (Fig. 4d). Out of the eight significant subsurface warming years only three negative IOD events (1988, 1998 and 1999) co-occurred with La Niña in the model (Fig. 4c). This further suggests that the La Niña like forcing is mainly responsible for EEIO warming. It is important to note that EEIO subsurface warming is extremely high when La Niña co-occurred with negative IOD events in the model.

Composite of surface and subsurface ocean temperature for above mentioned years and bias is shown in Fig. 5 over the TIO region. The model and observations showed warm SSTs above 28 °C over EIO region (Fig. 5a) in strong warm years composites. SST bias during strong warm years is similar to that of mean bias over the TIO region (Fig. 2a) with a slight warm bias over EEIO region (Fig. 5b). Further subsurface mean temperature bias (Fig. 2b) is high in CFSv2 during La Niña years over the EEIO (Fig. 5c). This warming is apparent in bias, which is supported by strong eastward current bias at equatorial region (Fig. 5d). Note that the ocean current bias for the composite analysis is biased on 1998, 1999, 2000, 2003, 2007 and 2011 as ECCO-2 data is available only from 1992. The subsurface warm bias over the EEIO is higher (~2 °C) than normal during these years (Fig. 6). Temperature bias at subsurface is stronger throughout the equator in strong warm

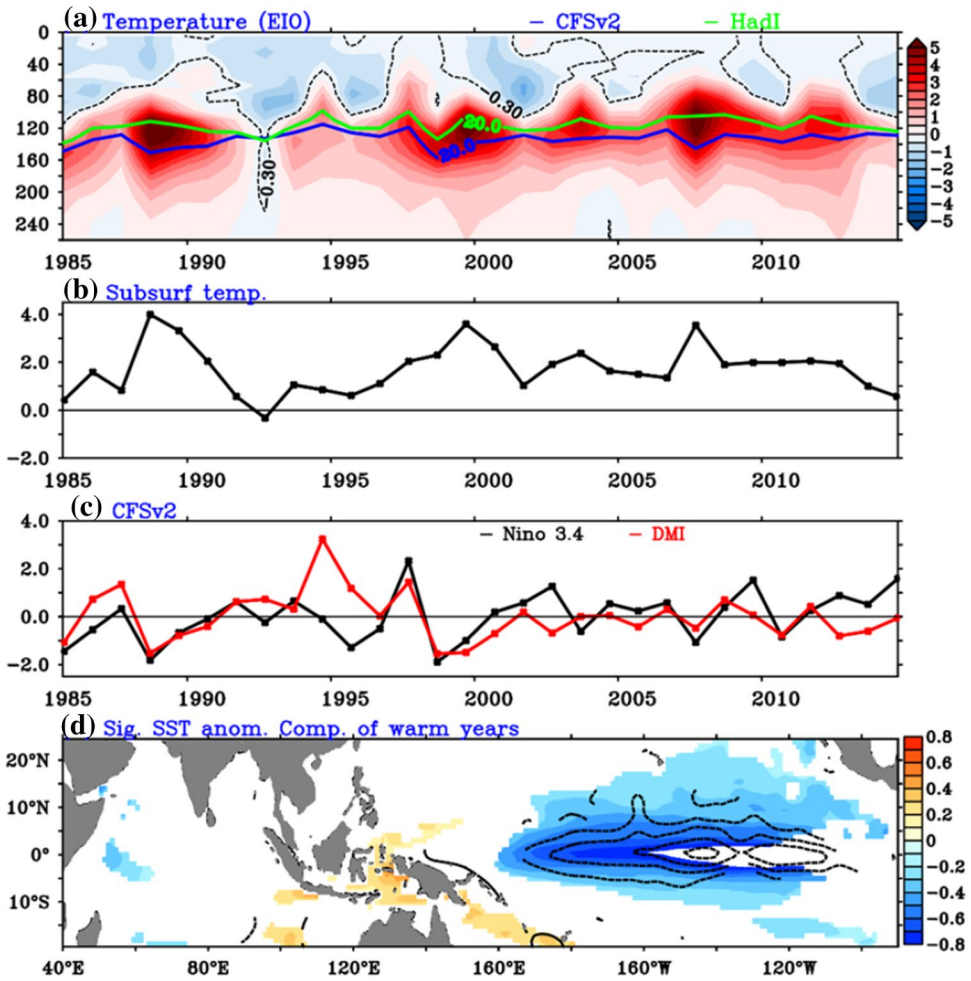

Fig. 4 **a** Depth–time plot (JJAS) of temperature bias averaged over EIO (90–100°E and 5°S–5°N) (*shaded* and contour; °C) and 20 °C isotherm (contour; CFSv2 *blue line* and HadI *green line*) **b** time series of subsurface temperature bias (average for 120–140 m; °C) over EEIO, **c** time series of CFSv2 Nino 3.4 region SST anomalies (*black line*) and DMI (*red line*; °C) and **d** strong warm year composite of SST anomalies (*shaded* CFSv2 and contours HadI EN4 product; °C) significant at 90% confidence level is displayed. Bias is calculated with respect to HadI EN4

bias years in the model compared to mean bias. It is noted that the structure of subsurface temperature and wind bias is same for both La Niña—negative IOD co-occurred years and La Niña only years.

Depth–longitude plot of temperature bias shows about 4 °C warm bias at 120–140 m depth over the EEIO region during strong warm years (Fig. 7a). This warm bias is higher than mean bias, highlighting the role of interannual variability in contributing to the mean subsurface bias. Anomalously strong eastward bias in currents up to 120 m depth is evident in strong warm years (Fig. 7b). This equatorial current bias supports subsurface warm bias in the EEIO by accumulating warm water and deepening the thermocline. Zonal current bias in the model averaged between 110 and 115°E during strong warm years (Fig. 7c) shows the robust westward current bias north of 12°S. This suggests that warm water inflow from the Indonesian through flow is high at surface and subsurface during the La Niña like years. Heat transport of the Indonesian through flow to Indian Ocean is in general higher during La Niña years (e.g., Vranes et al. 2002). Further enhanced downward motion of vertical velocity component up to a depth of 120 m is evident which supports subsurface warming (Fig. 7d). Our analysis suggests that subsurface warm bias is not highly influenced by El Niño forcing unlike atmospheric circulation elsewhere, but highly influenced by La Niña like forcing. It is found that during El Niño years subsurface temperature over EEIO is not highly influenced and there is no cooling effect (figure not shown). However, during La Niña or strong warm years subsurface warming is high in the coupled model. Further, composite years of strong warm temperature bias over the EIO (for May CFSv2 initial conditions from GODAS) suggests that contribution of initial conditions to subsurface warming bias over EEIO is not significant (figure not shown).

Association between atmospheric and oceanic parameters are analysed in JJAS long term mean and strong warm years composites. Composite of precipitation anomalies for the observations, model and bias are displayed in Fig. 8a–c. Zonal distribution of precipitation anomalies around the equator is opposite in the model as compared to the observations. Strong positive precipitation bias from 5 to 10°S over the eastern Indian Ocean region is apparent in the model. These differences in rainfall anomaly

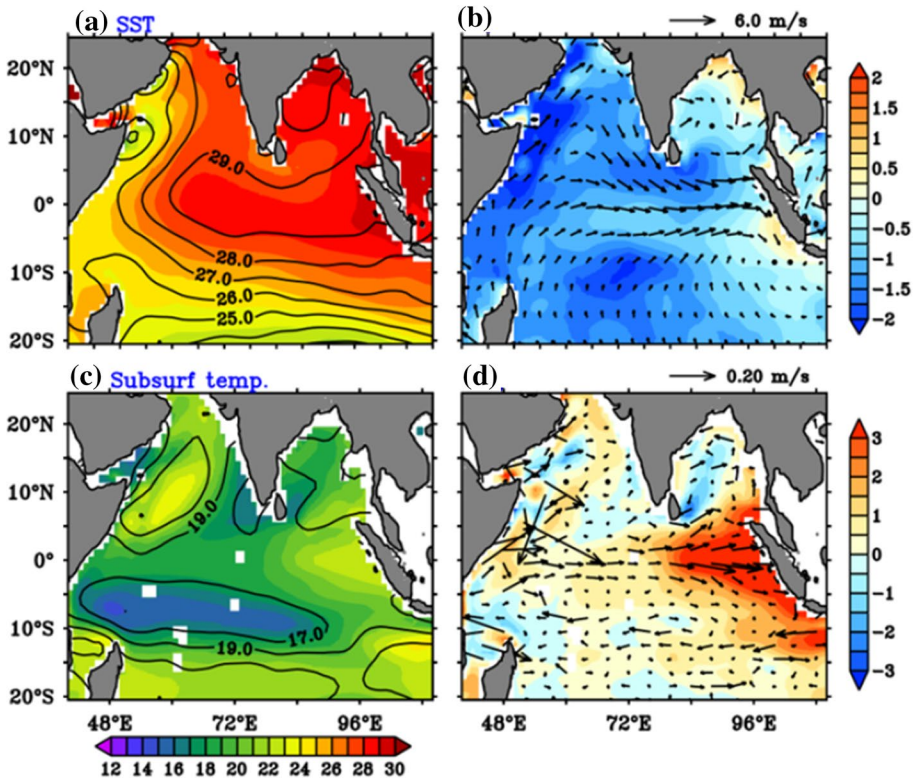

Fig. 5 Composite of strong warm years (JJAS): **a** SST (*shaded* CFSv2 and contour HadI EN4; °C) and **b** SST bias (*shaded*; °C) and surface winds bias (vectors; m/s), **c** subsurface temperature (average of 120–140 m) (*shaded*, CFSv2 and contour, HadI EN4; °C) and **d** bias for subsurface temperature (*shaded*; °C) and currents averaged over same depth (vectors; m/s)

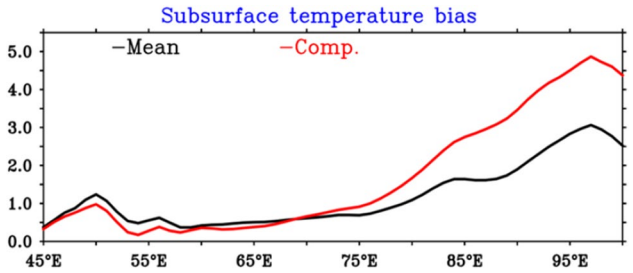

Fig. 6 Subsurface temperature bias (°C) averaged over 5°S–5°N and 120–140 m depth for annual mean (*black line*) and La Niña composite or maximum bias years (*red line*) during summer

pattern are consistent with surface wind bias with convergence (90–100°E and 10°S to equator) over the EEIO region (Fig. 5b), which in turn is favourable for surface and subsurface temperature bias over this region. Large scale circulation pattern associated with La Niña like events generally influences the EEIO and western Pacific region. Velocity potential at 200 hPa and divergent component of mean wind composites during strong warm years suggest that the model displays strong upper level divergence (200 hPa) over the Indo-western Pacific region and which slightly extended towards EEIO (southwest ward) region as compared to the observations (Fig. 8d, e). This upper level circulation difference between the observations and model is consistent with low level convergence over the EEIO region.

Anomalous Walker circulation composite in strong warm years along the equator between 5°S and 5°N over the Indo-Pacific region is shown in Fig. 9a–c. Consistent with cold SST anomalies associated with La Niña (Fig. 4d), subsidence over the central and eastern Pacific is noted in the observations and model. Strong ascending motion with low level convergence and upper level divergence in the western Pacific and EEIO region are evident during strong warm years. However, the model shows stronger upward motion and enhanced convection over the EEIO region as compared to the observations (Figs. 8c, e, 9c). This difference is also apparent in local Hadley circulation (averaged over 85–95°E) with strong ascending branch (from 10°S to equator and 1000 to 200 hPa) in the model around EEIO region unlike in the observations (Fig. 9d–f). On the other hand, bias in Hadley circulation shows downward motion over the head Bay of Bengal (15–25°N and from surface to 200 hPa) suggesting weak ascending branch in the model. Thus anomalous convergence over the eastern EIO during strong warm bias years is consistent with high rainfall and surface and subsurface temperature warming and low rainfall over the head Bay of Bengal (Figs. 8c, 9d–f). Krishnan et al. (2006) demonstrated that a higher than normal heat content over the EEIO due to deep thermocline or warm subsurface temperature could induce strong and sustained suppression of monsoon rainfall in some parts of India. Overall the misrepresentation of atmospheric teleconnections during La Niña like events to eastern Indian Ocean in

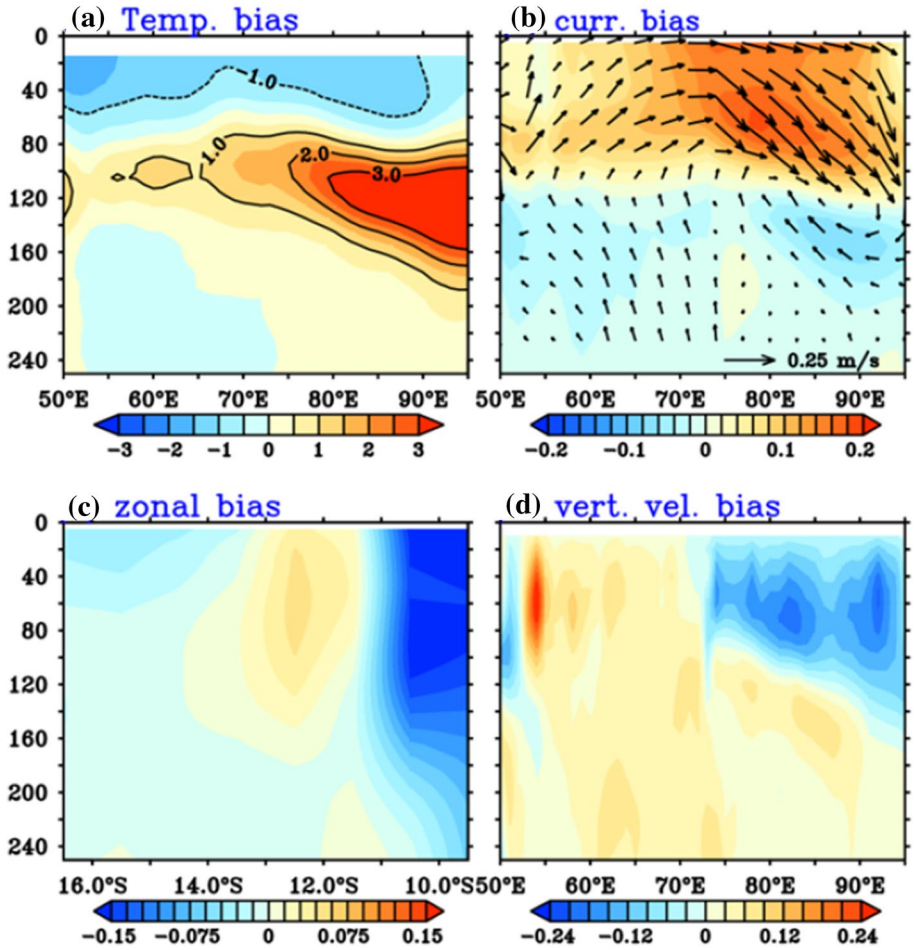

Fig. 7 Bias (JJAS) of upper 250 m depth–longitude plot (averaged over 3°S–3°N) for composite of strong warm years **a** temperature (*shaded* and contour; °C), **b** zonal current (*shaded*; m/s) and zonal and vertical currents (10^4) (vectors; m/s), **c** depth–latitude plot of zonal current (averaged over 110–115°E) (*shaded*; m/s) and **d** same as **a** but for vertical current (*shaded*; 10^4 m/s)

the model is mainly responsible for maximum warm subsurface bias over the EEIO region.

During summer of normal years, sea level pressure (SLP) displays positive (negative) bias over western (eastern) Indian Ocean (Fig. 10a). Consistent with SLP bias, CFSv2 shows westerly wind (850 hPa) bias over the equatorial region. Easterly winds bias over the equatorial western Pacific and westerly wind bias over the EIO supported the warm bias near the Maritime continent and regions such as EEIO. Net heat flux bias is positive over the EEIO unlike the regions away from the equator (Fig. 10c), this positive bias in net heat flux along with ocean dynamics caused for warm SST bias. Further, latent heat bias is low (ocean losing less heat to atmosphere) as compared to other regions and at the same time rainfall bias is high (Fig. 10c) due to local convergence of winds. Thus low evaporation may contribute for maintaining weak positive SST bias over the EEIO. During strong warm years the gradient of SLP bias is slightly high as compared to mean bias (Fig. 10b). Strong negative SLP bias over the northwest Pacific is apparent in the strong warm years. As a result of positive SLP bias in the western Indian Ocean and negative SLP bias in eastern Indian Ocean and northwest Pacific, winds over the EIO show strong westerly bias and which is higher in strong warm years than in mean or normal years. This equatorial wind bias has induced eastward current bias in the upper ocean causing subsurface warm bias by piling up of warm water in the east and by pushing warm water below. Net heat flux bias is positive and latent heat flux bias is low over the EIO during strong warm years and these biases are slightly higher compared to mean bias (Fig. 10d). Altogether, strong subsurface warm bias over the EEIO is evident during La Niña like years and has strong resemblance with climatological bias. This anomalous subsurface bias affects the upper ocean heat content and modulates local air-sea interactions.

Contribution of surface heat budget terms for JJAS mean and composite of strong subsurface warming years reveals that the heat flux term in the model contributes positively over EEIO region (Figure not shown) unlike in the observations. Most of the TIO region in model shows negative contribution of heat flux. Further zonal advection contributes positively over southern Indian Ocean (SIO) both in observations and model. But zonal advection over SIO is stronger than observations in model and it could influence the intrusion of warm waters from Pacific Ocean through

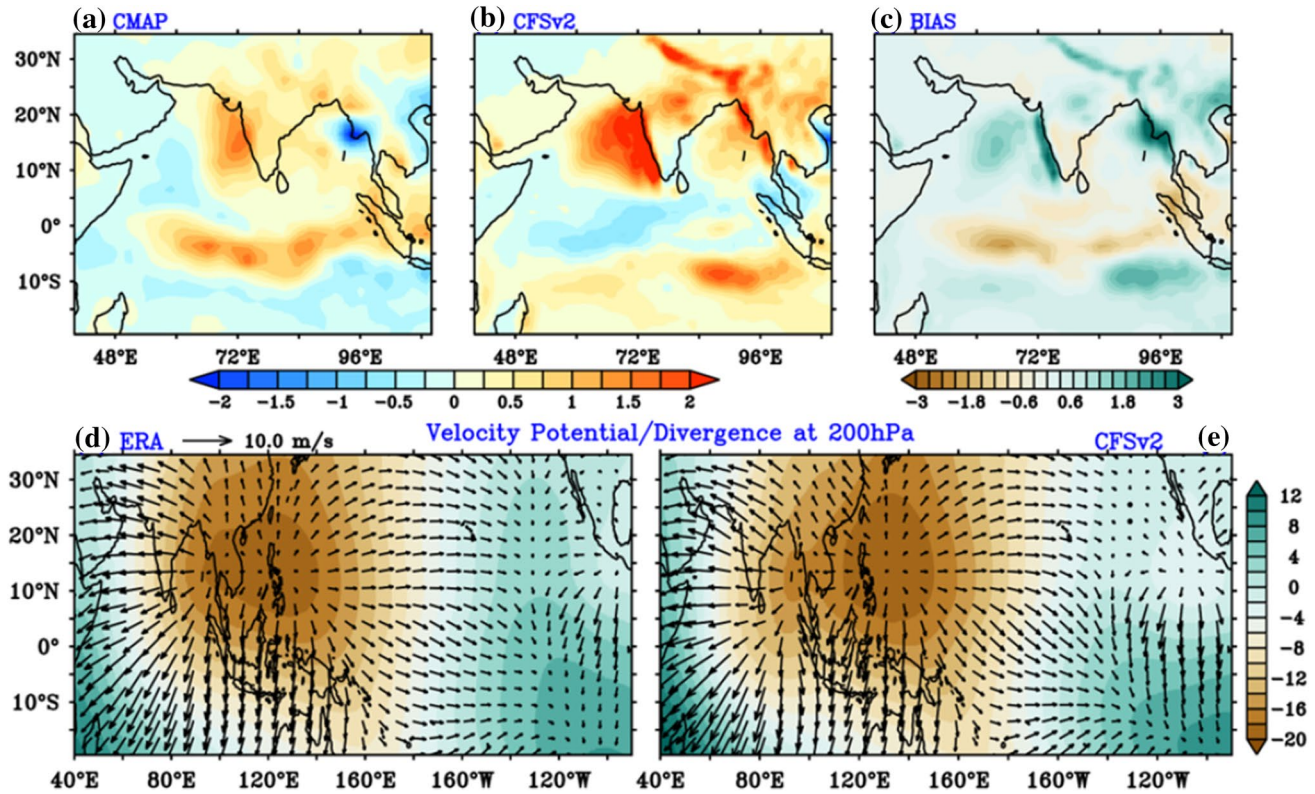

Fig. 8 Spatial pattern of JJAS composite of strong warm years: **a** CMAP precipitation anomalies (*shaded*; mm/day), **b** CFSv2 precipitation anomalies (*shaded*; mm/day), **c** bias (CFSv2—CMAP; mm/day), **d** ERA-interim velocity potential (*shaded*; 10^6 m^3/s) and divergence at 200 hPa (vectors; m/s) and **e** same as **d** but for CFSv2

Indonesian through flow (Chowdary et al. 2016b). Entrainment in the model contributes positively like in the observations with higher magnitudes. This positive contribution of entrainment indicates downwelling of surface waters over EEIO and causes subsurface warming. Chowdary et al. (2015, 2016a) have performed heat budget analysis and found that SST bias away from the equatorial region is highly influenced by latent heat flux and ocean dynamics play an important role in the equatorial region. Further to understand the processes associated with subsurface temperature bias, we have carried out subsurface heat budget analysis based on Halkides et al. (2011).

Subsurface heat budget terms for JJAS mean and composite of strong warming years suggest that zonal advection in model contributes positively in contrast to the observations over EEIO (Fig. 11c, d). This could enhance the accumulation of warm waters over the region due to positive contribution of zonal advection in model. Further vertical advection in model contributes positively unlike in the observations (Fig. 11g, h). This positive contribution of vertical advection over EEIO region reveals downwelling of warm waters over EEIO. Over all, both horizontal and vertical advection play an important role in generating strong subsurface temperature bias over the EEIO in CFSv2.

Figure 12 shows the depth-longitude plot of EIO temperature and current bias (with respect to observations) for Exp-1 and Exp-2 carried out using OGCM. It is evident that subsurface warm bias over the EEIO is much stronger when forced with CFSv2 winds. Induced by equatorial westerly winds in Exp-2, surface current shows eastward bias with strong downward motion in the EEIO caused for anomalous subsurface bias. This clearly provides evidence for the proposed mechanism that both horizontal and vertical current biases are responsible for the warm bias induced by strong EIO wind bias in CFSv2. Thus it is suggested that equatorial surface wind bias in CGCMs including CFSv2 and CMIP5 models need to be reduced for the better representation of subsurface or thermocline structure. In particular wind bias in CFSv2 originates from the large SLP bias.

5 Summary and discussion

The present study examined the upper ocean mean thermal structure biases in CFSv2 over the equatorial Indian Ocean during summer and its relation with interannual variability. In the tropical Indian Ocean region, maximum warm subsurface temperature mean bias greater than 3 °C is reported

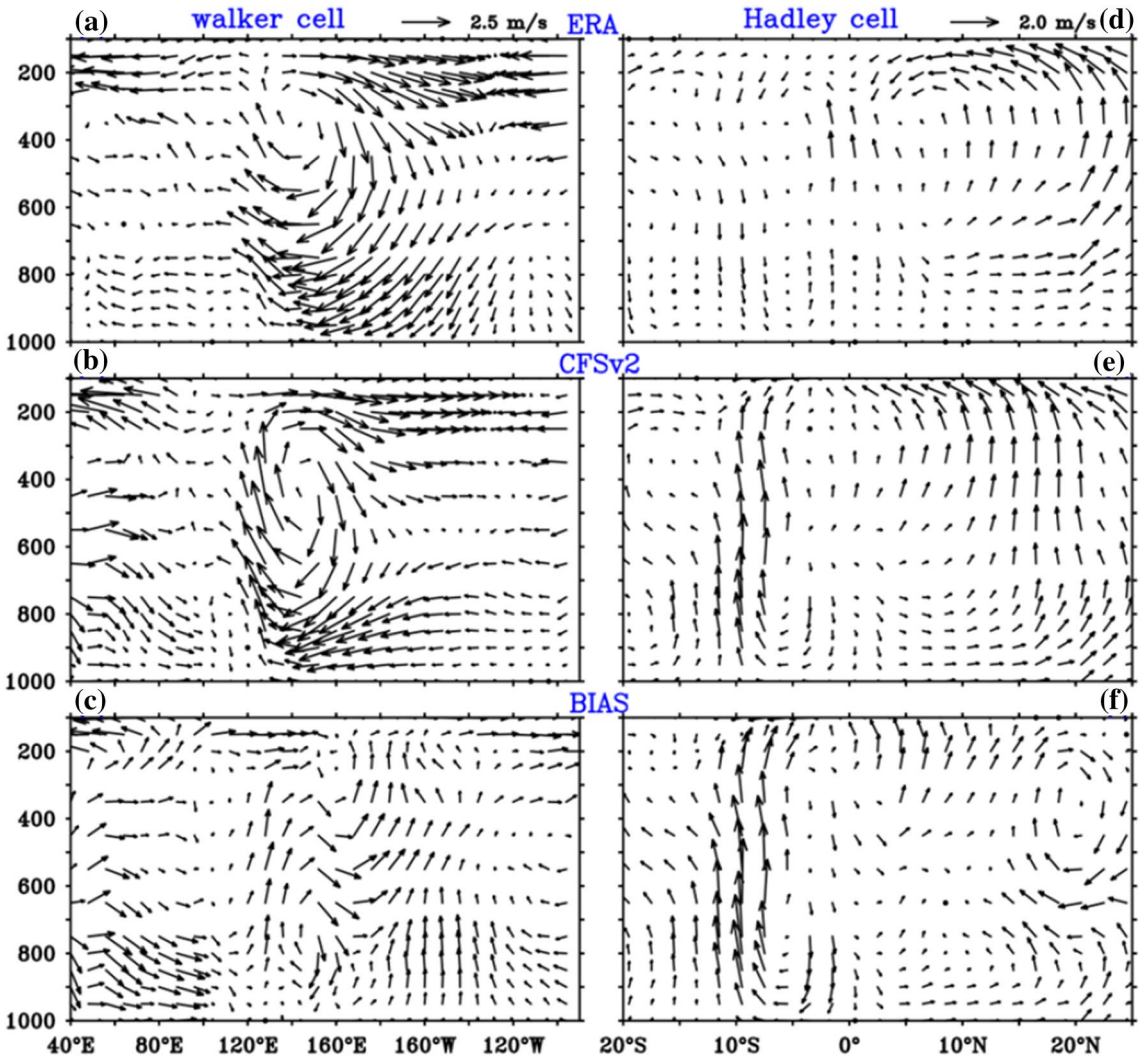

Fig. 9 Strong warm year composite Walker (zonal) circulation anomalies over Indo–Pacific region averaged between 5°S and 5°N **a** ERA, **b** CFSv2 and **c** bias (CFSv2 minus ERA). Hadley/Meriodional circulation (averaged over 85–95°E) over EIO region: **d** ERA, **b** CFSv2 and **c** bias (CFSv2 minus ERA) during JJAS. The vertical velocity (10^{-2} Pa s^{-1}) is taken with negative sign

in the EEIO region in CFSv2. Detailed analysis suggests that SLP gradient with positive (negative) bias in the western EIO (eastern EIO) supports westerly wind bias over the equatorial region during summer in CFSv2. This westerly wind bias induces strong eastward current bias in the upper 100 m over the EIO region, which accumulates warm water over the EEIO and punched down to subsurface with deep thermocline locally.

The role of interannual biases on the model mean bias is not known previously. In this study it is found that the model biases are not same from one year to another. Detailed analysis reveals that the maximum subsurface bias episodes over the EEIO are evident during La Niña like (both in developing and decay years) years and El Niño has little or no such impact on EEIO subsurface bias making an asymmetric EEIO response. Large scale forcing associated with La Niña like events is known to influence the Indian Ocean climate (e.g., Singh et al. 2013; Bansod 2011). Strong convergence of low level winds over the Maritime continent and EEIO associated with cooling over the equatorial central Pacific help to strengthen westerly wind bias over the EIO. This westerly wind bias in La Niña like composite is much stronger than mean wind bias. SLP gradient bias also enhanced during the strong warm years with positive SLP bias over western EIO and negative SLP bias over EEIO and parts of western Pacific. Corroborated by SLP biases, strong westerly bias in low level wind caused anomalous eastward current bias in the upper 100 m, which results for enhanced warm subsurface bias. Biases in atmospheric circulation associated with La Niña like events influence the ocean dynamics by modulating the ocean circulation

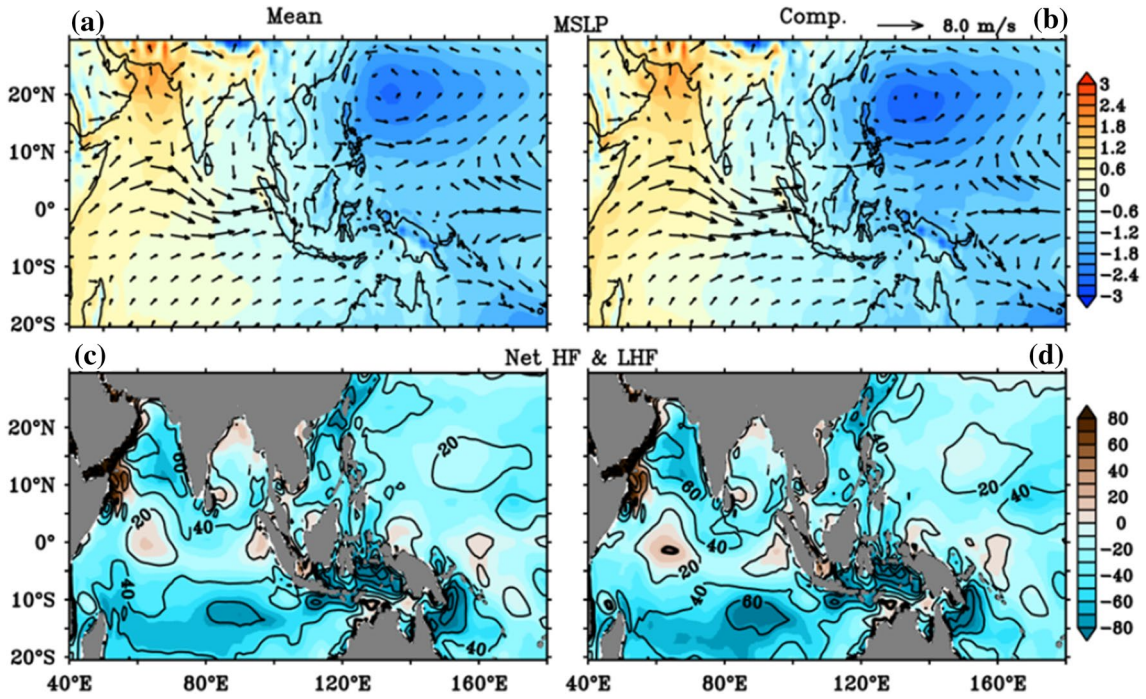

Fig. 10 JJAS bias **a** composite of normal years mean sea level pressure (MSLP) (*shaded*; hPa) and 850 hPa winds (vectors; m/s), **b** composite of strong warm years MSLP (*shaded*; hPa) and 850 hPa winds (vectors; m/s), **c** mean net heat flux (NHF) (*shaded*; w/m^2) and latent heat flux (LHF) (*contours*; w/m^2), and **d** La Niña years NHF (*shaded*; w/m^2) and LHF (*contours*; w/m^2). Winds and MSLP biases are with respect to ERA interim, and flux biases are based on the TropFlux

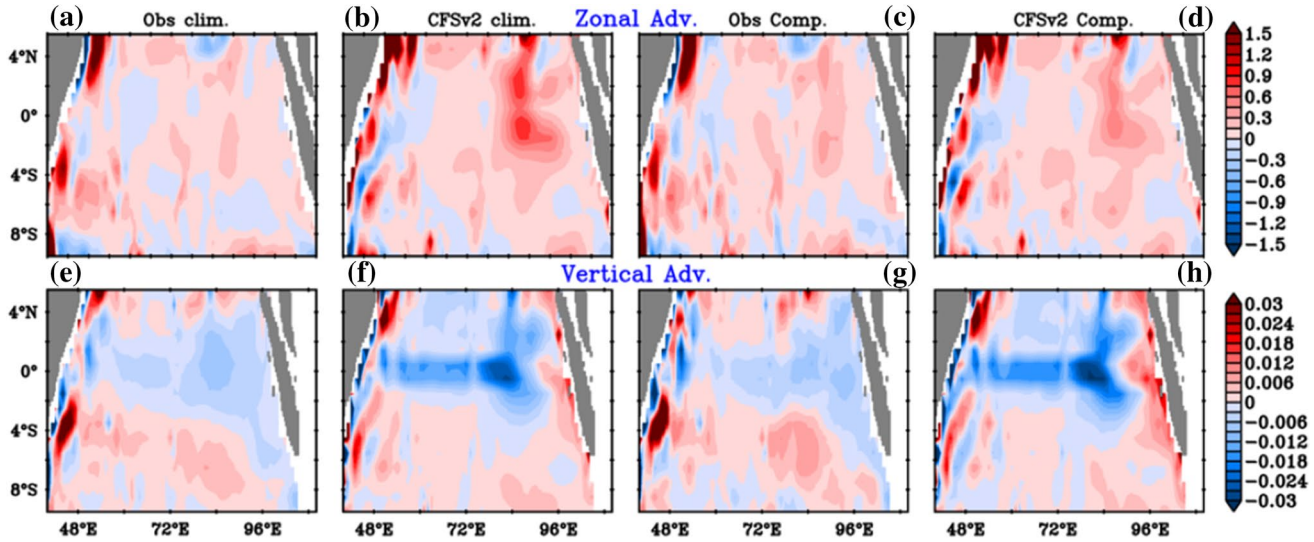

Fig. 11 Spatial pattern of subsurface heat budget terms of JJAS mean and composite of strong warm years for observations and model: **a**–**d** zonal advection contribution averaged over a depth of 120–140 m (*shaded*; °C) for mean of observation, model, composite of strong warming years for observations and model showed respectively. Similarly **e**–**h** for vertical advection

and thereby enhancing subsurface warm bias over the EEIO. Further analysis reveals that EEIO subsurface warming is higher during La Niña and negative IOD co-occurrence years in the model compared to La Niña only years. Structure of subsurface temperature and wind bias is same in both co-occurrence years and La Niña only years. Thus same mechanism is true for both cases in explaining the EEIO subsurface warming in the model.

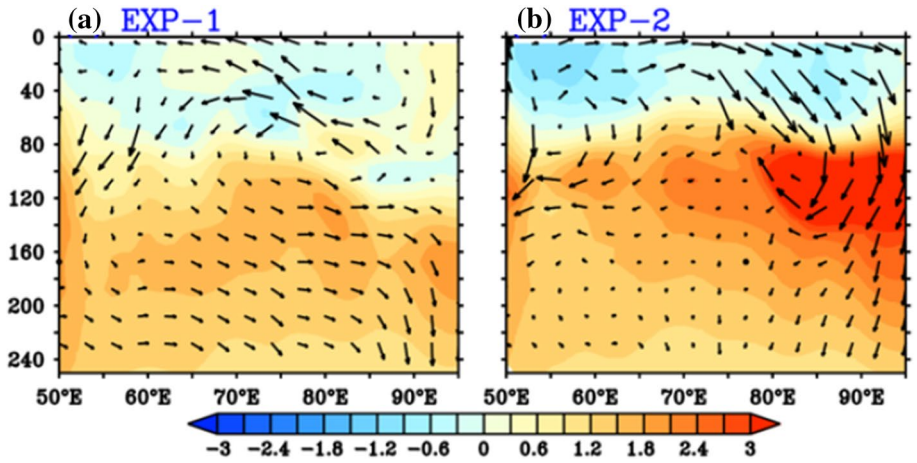

Fig. 12 Depth–longitude plot (JJAS) for upper 250 m (average over 5°S–5°N) bias of **a** Exp-1 temperature (*shaded*; °C) and zonal and vertical currents (10^4 m/s) (vectors; m/s), **b** same as **a** but for Exp-2

This study indicates that it is important to understand the ability of models in representing the tropical air-sea interactions properly and their impact on ocean biases. Strong warm bias associated with interannual events could contribute for mean bias in the model. Monsoon rainfall over many parts of India is influenced by La Niña like forcing. Westward shift in convective zone over the western Pacific associated with La Niña like forcing and SLP bias in the model are mainly responsible for biases in atmospheric circulation over Indo-western Pacific. OGCM simulations forced by strong warm years composite winds from CFSv2 displayed stronger subsurface warm bias over the EEIO compared to that forced by observed winds. Induced by EIO westerly winds, associated with La Niña like conditions in Pacific, surface current displays eastward bias with strong downward motion in the EEIO, resulting anomalous EEIO subsurface bias. This clearly indicates that horizontal and vertical current biases associated with surface wind bias results for the warm subsurface bias. This study highlights that equatorial surface wind bias in CGCMs (including CFSv2 and CMIP5 models) need to be reduced in order to obtain better subsurface or thermocline structure, which is important to maintain proper thermocline-SST feedback and air–sea interaction.

Acknowledgements We thank Director, ESSO-IITM for support. We have used (Hadley EN4.1.1) temperature data from http://www.metoffice.gov.uk/hadobs/en4/download-en4-1-1.html, ECCO data from http://www.ecco-group.org, and ERA interim data from http://www.ecmwf.int/en/research/climate-reanalysis/era-interim. We sincerely thank the anonymous reviewers for their valuable comments that helped us to improve the manuscript. Figures are prepared in PyFerret.

References

Anderson DM, Overpeck JT, Gupta AK (2002) Increase in the Asian southwest monsoon during the past four centuries. Science 297:596–599

Balaguru K, Ruby Leung L, Yoon JH (2013) Oceanic control of Northeast Pacific hurricane activity at interannual timescales. Environ Res Lett 8(4):044009. doi:10.1088/1748-9326/8/4/044009

Ballester J, Burns JC, Cayan D, Nakamura Y, Uehara R, Rodó X (2013) Kawasaki disease and ENSO-driven wind circulation. Geophys Res Lett 40:2284–2289. doi:10.1002/grl.50388

Bansod SD (2011) Interannual variability of convective activity over the tropical Indian Ocean during the El Niño/La Niña events. Int J Remote Sens 32(19):5565–5582

Brown JN, Sen Gupta A, Brown JR, Muir LC, Risbey JS, Whetton P, Zhang X, Ganachaud A, Murphy B, Wijffels SE (2013) Implications of CMIP3 model biases and uncertainties for climate projections in the western tropical Pacific. Clim Change. doi:10.1007/s10584-012-0603-5

Chang P, Yamagata T, Schopf P, Behera SK, Carton J, Kessler WS, Meyers G, Qu T, Schott F, Shetye SR, Xie S-P (2006) Climate fluctuations of tropical coupled systems—the role of ocean dynamics. J Clim 19:5122–5174

Chaudhari HS, Pokhrel S, Mohanty S, Saha SK (2013) Seasonal prediction of Indian summer monsoon in NCEP coupled and uncoupled model. Theor Appl Climatol 114:459–477

Cherchi A, Navarra A (2007) Sensitivity of the Asian summer monsoon to the horizontal resolution: differences between AMIP-type and coupled model experiments. Clim Dyn 28:273–290

Chowdary JS, Parekh A, Sayantani O, Gnanaseelan C (2015) Role of upper ocean processes in the seasonal SST evolution over tropical Indian Ocean in Climate Forecasting System. Clim Dyn. doi:10.1007/s00382-015-2478-4

Chowdary JS, Parekh A, Ojha S, Gnanaseelan C, Kakatkar R (2016a) Impact of upper ocean processes and air–sea fluxes on seasonal SST biases over the tropical Indian Ocean in the NCEP Climate Forecasting System. Int J Clim 4336:188–207. doi:10.1002/joc

Chowdary JS, Anant Parekh, Srinivas G, Gnanaseelan C, Fousiya TS, Rashmi K, Roxy MK (2016b) Processes associated with the tropical Indian Ocean subsurface temperature bias in a coupled model. J Phys Ocean. doi:10.1175/JPO-D-15-0245.1

De S, Hazra A, Chaudhari HS (2015) Does the modification in "critical relative humidity" of NCEP CFSv2 dictate Indian mean summer monsoon forecast? Evaluation through thermodynamical and dynamical aspects. Clim Dyn. doi:10.1007/s00382-015-2640-z

Dee D et al (2011) The ERA-interim reanalysis: configuration and performance of the data assimilation system. Quart J R Meteor Soc 137: 553–597

Good SA, Martin MJ, Rayner NA (2013) EN4: quality controlled ocean temperature and salinity profiles and monthly objective

analyses with uncertainty estimates. J Geophys Res Ocean 118:6704–6716. doi:10.1002/2013JC009067
Griffies SM (2012) Elements of the modular ocean model (MOM): 2012 release (GFDL Ocean group technical report no. 7. GFDL Ocean group technical report no. 7. NOAA/Geophysical Fluid Dynamics Laboratory, Princeton
Griffies S, Harrison MJ, Pacanowski RC, Anthony R. (2004) A technical guide to MOM4, GFDL Ocean group, technical report no. 5, NOAA/Geophysical Fluid Dynamics Laboratory, Princeton, p 342
Halkides DJ, Lee T, Kida S (2011) Mechanisms controlling seasonal mixed-layer temperature and salinity of the Indonesian seas. Ocean Dyn 61:481–495. doi:10.1007/s10236-010-0374-3
Jiang X, Yang S, Li J, Li Y, Hu H, Lian Y (2013) Variability of the Indian Ocean SST and its possible impact on summer western North Pacific anticyclone in the NCEP Climate Forecast System. Clim Dyn 41:2199–2212
Keenlyside NS, Latif M (2007) Understanding equatorial Atlantic interannual variability. J Clim 20:131–142
Kirtman B, Vecchi GA (2011) Why climate modelers should worry about atmospheric and oceanic weather. In: Chang C-P, Ding Y, Lau N-C, Johnson RH, Wang B, Yasunari T (eds) The global monsoon system: research and forecast, 2nd edn. World scientific series on Asia-Pacific weather and climate, vol 5. World Scientific Publication Company, Singapore, pp 511–524
Krishnamurthy V, Kinter JL (2003) The Indian monsoon and its relation to global climate variability. Global climate. Rodó X, Comín FA (eds) Springer, Berlin, 186–236
Krishnamurthy V, Kirtman B (2003) Variability of the Indian Ocean: relation to monsoon and ENSO. Quart J R Meteorol Soc 129: 1623–1646
Krishnan R, Ramesh KV, Samala BK, Meyers G, Slingo JM, Fennessy MJ (2006) Indian Ocean–monsoon coupled interactions and impending monsoon droughts. Geophys Res Lett 33:L08711. doi:10.1029/2006GL025811
Large WG, Danabasoglu G (2006) Attribution and impacts of upper-ocean biases in CCSM3. J Clim 19:2325–2346
Levitus S, Boyer TP, Conkright ME, O' Brien T, Antonov J, Stephens C, Stathoplos L, Johnson D, Gelfeld R (1998) NOAA Atlas NESDIS 18,World Ocean Database 1998: volume 1: introduction. US Gov. Printing Office, Washington, DC, p 346
Li G, Xie S-P (2012) Origins of tropical-wide SST biases in CMIP multi-model ensembles. Geophys Res Lett 39:L22703. doi:10.1029/2012GL053777
Li G, Xie S-P (2014) Tropical biases in CMIP5 multimodel ensemble: the excessive equatorial Pacific cold tongue and double ITCZ problems. J Clim 27:1765–1780
Li G, Xie S-P, Du Y (2015a) Monsoon-induced biases of climate models over the tropical Indian Ocean. J Clim 28:3058–3072
Li G, Xie S-P, Du Y (2015b) Climate model errors over the south Indian Ocean thermocline dome and their effect on the basin mode of interannual variability. J Clim 28:3093–3098
Li G, Xie S-P, Du Y (2016) A robust but spurious pattern of climate change in model projections over the tropical Indian Ocean. J Clim 29:5589–5608
Lin JL (2007) The double-ITCZ problem in IPCC AR4 coupled GCMs: ocean–atmosphere feedback analysis. J Clim 20:4497–4525
Luo J-J, Masson S, Roeckner E, Madec G, Yamagata T (2005) Reducing climatology bias in an ocean–atmosphere CGCM with improved coupling physics. J Clim 18:2344–2360
Luo J-J, Sasaki W, Masumoto Y (2012) Indian Ocean warming modulates Pacific climate change. Proc Natl Acad Sci USA 109(46):18701–18706
McCreary JP, Kundu PK, Molinari R (1993) A numerical investigation of dynamics, thermodynamics and mixed-layer processes in the Indian Ocean. Prog Oceanogr 31:181–244
Pant GB, Rupa Kumar K (1997) Climates of South Asia. Wiley, Chichester, p 320
Pokhrel S, Rahaman H, Parekh A, Saha SK, Dhakate A, Chaudhari HS, Gairola RM (2012) Evaporation–precipitation variability over Indian Ocean and its assessment in NCEP Climate Forecast System (CFSv2). Clim Dyn 39:2585–2608
Preethi B, Sabin TP, Adedovin JA, Ashok K (2015) Impacts of the ENSO Modoki and other tropical Indo-Pacific climate-drivers on African rainfall. Sci Rep. doi:10.1038/srep16653
Ramu DA, Sabeerali CT, Chattopadhyay R, Rao DN, George G, Dhakate AR, Salunke K, Srivastava A, Rao SA (2016) Indian summer monsoon rainfall simulation and prediction skill in the CFSv2 coupled model: impact of atmospheric horizontal resolution. J Geophys Res Atmos 121:2205–2221. doi:10.1002/2015JD024629
Ruiz JE, Cordery I, Sharma A (2005) Integrating ocean subsurface temperatures in statistical ENSO forecasts. J Clim 18(17):3571–3586. doi:10.1175/JCLI3477.1
Saha S, Nadiga S, Thiaw C, Wang J, Wang W, Zhang Q, van den Dool HM, Pan HL, Moorthi S, Behringer D, Stokes D, Peña M, Lord S, White G, Ebisuzaki W, Peng P, Xie P (2006) The NCEP climate forecast system. J Clim 19:3483–3517
Saha S et al (2010) The NCEP climate forecast system reanalysis. Bull Am Meteor Soc 91:1015–1057. doi:10.1175/2010BAMS3001.1
Saha S, Moorthi S, Wu X, Wang J, Nadiga S, Tripp P, Pan HL, Behringer D, Hou YT, Chuang HY, Mark I, Ek M, Meng J, Yang R (2014) The NCEP climate forecast system version 2. J Clim 27:2185–2208. doi:10.1175/JCLI-D-12-00823.1
Saha SK, Sujith K, Pokhrel S, Chaudhari HS, Hazra A (2016) Predictability of global monsoon rainfall in NCEP CFSv2. Clim Dyn 47(5–6):1693–715
Saji NH, Goswami BN, Vinayachandran PN, Yamagata T (1999) A dipole mode in the tropical Indian Ocean. Nature 401:360–363
Schott FA, McCreary JP (2001) The monsoon circulation of the Indian Ocean. Prog Oceanogr 51:1–123
Schott FA, Xie SP, McCreary JP (2009) Indian Ocean circulation and climate variability. Rev Geophys 47:RG1002. doi:10.1029/2007RG000245
Sengupta D, Senan R, Murty VSN, Fernando V (2004) A biweekly mode in the equatorial Indian Ocean. J Geophys Res 109:C10003. doi:10.1029/2004JC002329
Sengupta D, Senan R, Goswami BN (2007) Intraseasonal variability of equatorial Indian Ocean zonal currents. J Clim 20:3036–3055
Shankar D, Vinayachandran PN, Unnikrishnan AS (2002) The monsoon currents in the north Indian Ocean. Prog Oceanogr 52:63–120
Singh P, Chowdary JS, Gnanaseelan C (2013) Impact of prolonged La Niña Events on the Indian Ocean with a special emphasis on Southwest Tropical Indian Ocean SST. Glob Plan Change 100: 28–37
Sreenivas P, Gnanaseelan C (2014) Impact of oceanic processes on the life cycle of severe cyclonic storm Jal. IEEE Geosci Remote Sens Lett 11:519–523. doi:10.1109/LGRS.2013.2271512
Tao W, Huang G, Hu K, Gong H, Wen G, Liu L (2015) A study of biases in simulation of the Indian Ocean basin mode and its capacitor effect in CMIP3/CMIP5 models. Clim Dyn. doi:10.1007/s00382-015-2579-0
Vincent EM, Emanuel KA, Lengaigne M, Vialard J, Madec G (2014) Influence of upper ocean stratification interannual variability on tropical cyclones. J Adv Model Earth Syst 6:680–699. doi:10.1002/2014MS000327
Vranes K, Gordon AL, Ffield A (2002) The heat transport of the Indonesian through flow and implications for the Indian Ocean heat

budget. Deep Sea Res Part II 49(7):1391–1410. doi:10.1016/S0967-0645(01)00150-3

Wunsch C, Heimbach P (2013) Dynamically and kinematically consistent global ocean circulation and ice state estimates. In: Sielder G, Griffies SM, Gould J, Church JA (eds) Ocean circulation and climate: a 21st century perspective. International Geophysics Series, vol 103. Academic Press, Oxford, pp 553–579. doi:10.1016/b978-0-12-391851-2.00021-0

Wyrtki K (1973) An equatorial jet in the Indian Ocean. Science 181:262–264

Xie P, Arkin PA (1997) Global precipitation: a 17-year monthly analysis based on gauge observations, satellite estimates, and numerical model outputs. Bull Am Meteorol Soc 78:2539–2558

Xie S-P, Annamalai H, Schott FA, McCreary JP (2002) Structure and mechanisms of South Indian Ocean climate variability. J Clim 15:864–878

Yamagata T, Behera SK, Luo JJ, Masson S, Jury MR, Rao SA (2004) Coupled ocean-atmosphere variability in the tropical Indian Ocean. In: Wang C, Xie SP, Carton A (eds) Earth's climate: the ocean–atmosphere interaction. Geophysical monograph, vol 147. American Geophysical Union, Washington DC, pp 189–211